




Evaluation of the impact of urban expansion and hyperconcentrated flow generation in a dry creek

Angel Gabriel Escobar Alama, Bachelor¹ , Nicolas Josias Castro Camacho, Student² , and Pedro Christopher Rau Lavado, PhD³ 

^{1,2,3}Universidad de Ingenieria y Tecnologia, Peru, angel.escobar@utec.edu.pe, nicolas.castro@utec.edu.pe, prau@utec.edu.pe

Abstract – *Hyperconcentrated flows are complex phenomena frequently linked to disasters in urban settlements. To comprehend the entirety of disaster hazards, it is crucial to adopt a broad perspective that encompasses environmental variables delineating the impact of imperviousness in stream areas, a common occurrence in urban expansion. The study was carried out in the 8.4 km² California dry creek in Chosica, Lima, Peru, and had the following objectives: 1) identify the most appropriate remote sensing products for mapping urban sprawl and imperviousness and their relationship to watershed hydrologic properties; 2) analyze hyperconcentrated storm flow hydrographs and their direction over the California watershed with a meteorological approach for the theoretical, 2013 and 2022 scenarios; and 3) estimate the rate of sediment generation in the watershed through the MUSLE method for the theoretical, 2013 and 2022 scenarios. The Normalized Difference Building Index (NDBI) was used to detect built-up areas between 2013 and 2022; and the Normalized Difference Vegetation Index (NDVI) and the Bare Soil Index (BSI) were proposed for a more accurate representation of area conditions.*

Peak flows were also evaluated using variations of the rational method, adapted to the study area. Soils were characterized, and critical erosion zones were identified using the MUSLE method and based on field reconnaissance. The results revealed the relative impact of imperviousness on the increase of hyperconcentrated flow peaks, both in magnitude and time of occurrence. It is highlighted that the widely used Normalized Difference Building Index (NDBI) does not adequately represent urban growth, confirming its limitations for desertic areas. These findings emphasize the importance of addressing imperviousness as a component of urban development, its negative effects on land-use planning, and the opportunity to adopt complementary nature-based solutions.

Keywords: *Remote sensing, hyperconcentrated flows, urban hydrology, environmental risk*

I. INTRODUCTION

Urban expansion around dry streams and creeks has been common since the 1970s in Lima surroundings because of socio-economic issues, which forced millions of people to move as an internal migration to the Peruvian capital city. In a desertic context, it was relatively easy to occupy great areas where most years are dry, but most of those areas are located in high flood-prone risk zones. This is because of the impacts of the El Niño phenomenon exacerbating precipitation and streamflow and worsening over steep Andean gradients [1]. Hyperconcentrated flows are distinguished as complex phenomena, and it is important to understand the associated

disaster hazard in its totality. This requires knowledge of the effect of stream and floodplain imperviousness, a common practice in urban development and expansion [2].

The use of remote sensing in mapping urban growth and diverse ecosystems in arid and coastal areas presents a challenge due to surface coloration and textures in a narrow range of detection. There are a variety of indices that can adequately identify under other conditions [3].

The Normalized Difference Vegetation Index (NDVI) is a useful index for identifying areas with vegetation, as well as water bodies, bare soil, and others; however, this can be unstable due to variation in soil color, soil moisture, and soil saturation [4]. In NDVI, values very close to zero may represent urban surfaces, whose interpretation should be complemented with indices such as the Normalized Difference Building Index (NDBI) and the Bare Soil Index (BSI), where positive values are indicators of urban or artificial surfaces [5]. NDVI is also affected by differential soil characteristics, geomorphology, and land use and is an effective indicator of vegetation growth pattern and density [6]. Therefore, it is a relevant index to identify vegetated areas in the lower watershed as well as to differentiate these areas from the urban surface.

BSI is formed by integrating the blue, red, near infrared and shortwave infrared spectral bands to detect changes in the earth's surface. The combination of the shortwave infrared and red band is used to measure the mineral composition of the soil, while the blue and near infrared spectral bands are used to highlight the presence of vegetation [7]. The use of BSI and NDVI allows a more accurate identification of soil classes in the California watershed, therefore, in this study they are used in a complementary manner to ensure a better recognition of surfaces.

II. STUDY SITE

The California dry creek is located in the district of Lurigancho-Chosica, in Lima, Peru. It has an area of 8.4 km², belonging to the Rimac River watershed. Its geological composition primarily consists of fractured and altered intrusive rocks, with substantial rocky block deposits dominating the upper section, while proluvial-alluvial deposits, also containing large blocks, prevail in the middle and lower sections [8]. The California watershed has a mean slope of 52.8% and a hypsometric curve with a slight concave

form, indicating the sedimentary production. The main stream has a length of 5.13 km and a slope of 13.7%.

To study the impact of imperviousness and land use and cover characterization, a field trip was conducted in July 2023, in which infiltration tests were carried out with a Minidisk Infiltrometer with soil samplings around two sites: M1 and M2, as shown in Fig. 1, and also drone overflights for aerial recognition in Fig. 2.

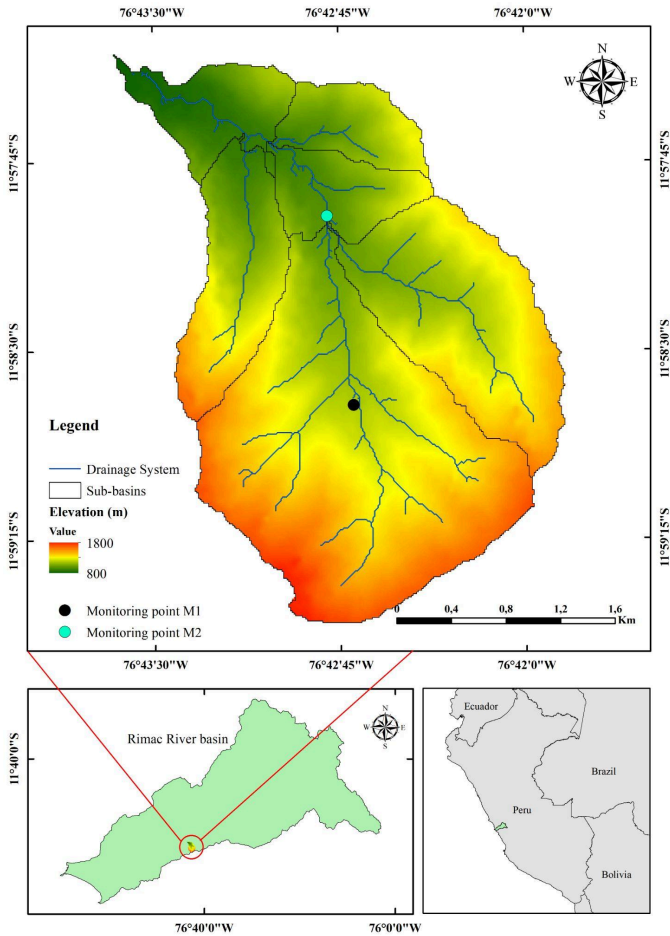


Fig. 1. California dry creek, Lurigancho-Chosica, Lima, Peru. Elevation range obtained from ALOS Palsar Digital Elevation Model.

III. METHODS

A. Mapping the change in soil imperviousness.

Google Earth Engine was used to obtain Landsat 5, 8, and 9 images between the years 2000 and 2023 with cloud cover less than 20%. Subsequently, NDVI, NDBI, and BSI indices were calculated within the watershed. Spectral indices were used in this research because they have shown important advances in mapping, estimation, land change detection, urban dynamics monitoring and other applications [9]. In addition, the indices

are tools that allow scalability and extraction of quantitative information from the study area [9].



Fig. 2 Panoramic downstream view (top), a plan view of shanty towns configuration (middle) and field work by UTEC students with infiltration tests and soil samples (bottom).

Equations (1), (2), and (3) represent the equations for NDVI, NDBI, and BSI, respectively, where SWIR represents the Shortwave Infrared band, NIR the Near Infrared band, Red the red band, and Blue the blue band.

Normalized Difference Vegetation Index (NDVI) equation:

$$NDVI = \frac{NIR - Red}{NIR + Red}. \quad (1)$$

Normalized Difference Building Index (NDBI) equation:

$$NDBI = \frac{SWIR - NIR}{SWIR + NIR}. \quad (2)$$

Bare Soil Index (BSI) equation:

$$BSI = \frac{(SWIR + Red) - (NIR + Blue)}{(SWIR + Red) + (NIR + Blue)}. \quad (3)$$

A visual inspection of the watershed was conducted in the field to identify predominant surfaces in the study area. Figure 2 displays surface characteristics in the California watershed obtained through visual and drone inspection. Additionally, the Global Land Cover (GLC-FAO) gridded product [10] was utilized to classify soil types within the watershed, serving as a baseline for the study area. Thus, the NDVI and BSI indices were used to recognize the following soil classes, which were identified in the field trip and complemented with the GLC-FAO baseline: sparse vegetation, bare soil, cropland, grassland and artificial surfaces.

Based on the evolution of the BSI index, the years 2013 and 2022 from Landsat 8 were identified as turning points; hence, impermeability was analyzed for these years using QGIS 3.28 software. Additionally, a theoretical scenario (NDVI) map was generated, depicting the absence of artificial surfaces in the middle and lower watershed, akin to conditions before the 1970s, displaying the vegetation classes identified in the area. Subsequently, the runoff coefficient was calculated for the isochrones in the theoretical, 2013 and 2022 scenarios. This information was used to calculate the hyperconcentrated flow hydrograph. Fig. 3 shows the methodological diagram followed in this research.

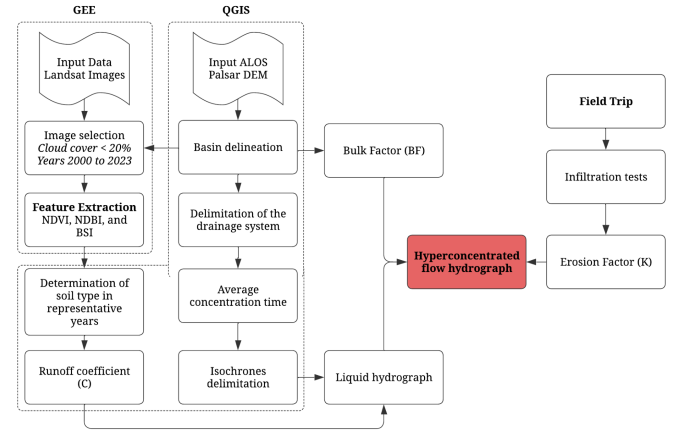


Fig. 3 Methodological scheme and used tools (GEE: Google Earth Engine, QGIS: Quantum Geographical Information System).

B. Estimation of hyperconcentrated flow hydrograph considering storm direction.

The hyperconcentrated flow hydrograph was estimated according to the direction of the storm, based on the meteorological behavior of precipitation events: “a downstream event” from the upper to the lower watershed (most common) and “an upstream event” in the opposite direction, for the years 2013 and 2022.

A rainfall intensity of 4 hours of duration was considered for a 25-year return period equivalent to 4.6 mm/hr [11]. As a reference, a strong total rainfall event of 33 mm occurred on 5th april 2017 during El Niño Costero [12].

Flow rates calculation was carried out using the modified rational method through isochrones [13], using runoff coefficients from the coverage estimation and spectral indices. The time of concentration of the watershed was estimated at 2 hours by an average of 18 empirical methods using the R hydRopUrban package [14, 15], which led to the subdivision of the watershed into four isochrone areas, each considering a 30-minute time interval according to the storm advance.

Hyperconcentrated flow (Q_{hf}) hydrographs were estimated by using a bulk factor (BF), which depends on a volumetric concentration of sediments “cv” around 0.25 for the events that occurred: $1/(1 - cv)$. The equation for hyperconcentrated flow is shown in (4).

$$Q_{hf} = \frac{c \cdot i \cdot A}{3.6} \cdot BF. \quad (4)$$

Where c is the runoff coefficient, i is the rainfall intensity (mm/hr), A is the area (km²).

For 4 isochrone areas:

$$\begin{aligned}
 Q_1 &= 0 \\
 Q_2 &= \frac{(c_1 \cdot A_1) \cdot BF \cdot i}{3.6} \\
 Q_3 &= \frac{(c_1 \cdot A_1 + c_2 \cdot A_2) \cdot BF \cdot i}{3.6} \\
 Q_4 &= \frac{(c_1 \cdot A_1 + c_2 \cdot A_2 + c_3 \cdot A_3) \cdot BF \cdot i}{3.6} \\
 Q_5 &= \frac{(c_1 \cdot A_1 + c_2 \cdot A_2 + c_3 \cdot A_3 + c_4 \cdot A_4) \cdot BF \cdot i}{3.6} \\
 Q_6 &= \frac{(c_2 \cdot A_2 + c_3 \cdot A_3 + c_4 \cdot A_4) \cdot BF \cdot i}{3.6} \\
 Q_7 &= \frac{(c_3 \cdot A_3 + c_4 \cdot A_4) \cdot BF \cdot i}{3.6} \\
 Q_8 &= \frac{(c_4 \cdot A_4) \cdot BF \cdot i}{3.6} \\
 Q_9 &= 0
 \end{aligned} \tag{5}$$

A_j is the area for the j -region. c_i is the runoff coefficient for the j -region. BF and i are constants for each isochrone.

C. Erosion rate estimation

An estimation of the erosion rate was carried out using the MUSLE method [16]. For this method, the ALOS Palsar Digital Elevation Model (DEM) was used to calculate the topographic factor (LS) of the watershed. Next, the soil erodibility (K) value was calculated through soil texture obtained from field samples and then analyzed in the soil laboratory. Sand, silt, and clay content were 72.9%, 23.6%, and 3.5%, respectively, for M1 (loamy sand) and 89.3%, 8.3%, and 2.4%, respectively, for M2 (sand), and some empirical relationships were considered and compiled in [17]. The soil textural triangle is shown in Fig. 4. The sedimentation rate towards the hydrographic network was calculated, and, finally, the information obtained from the liquid hydrograph was used to estimate the erosion generated during the storm event. The equation (6) shows the relationship to obtain the ratio of sediment to the hydrographic network.

$$Y = 11.8 \cdot (Q \cdot q_p)^{0.56} \cdot K \cdot LS \cdot C \cdot P \tag{6}$$

Y is the sediment rate to the hydrographic network (t). Q is the volume of runoff (m^3). q_p is the peak discharge ($m^3 \cdot s^{-1}$). K is the soil erodibility factor ($t \cdot h \cdot MJ^{-1} \cdot mm^{-1}$). LS is the topographic factor (dimensionless). C is the cover management factor (dimensionless). P is the support practice factor (dimensionless). For arid areas C and P are "1" due to lack of vegetation and soil conservation practices. The data for MUSLE equation was processed in R and QGIS.

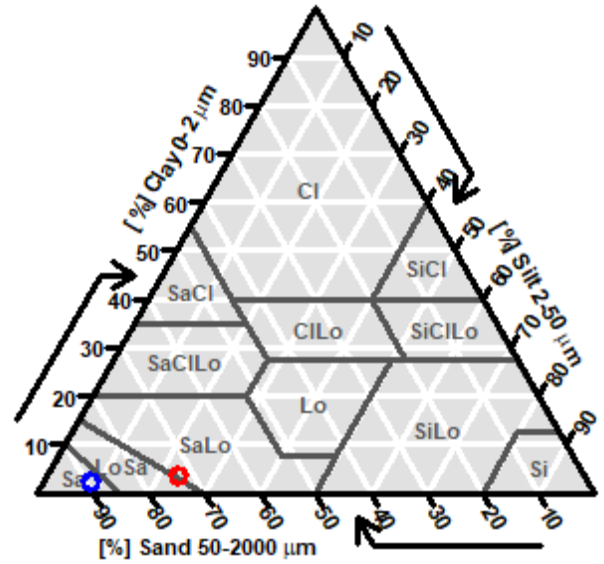


Fig. 4. Soil texture triangle of soil samples M1 (red) and M2 (blue).

IV. RESULTS

For California watershed conditions, it was found that BSI values greater than 0 and NDVI values in the range of 0.075 to 0.125 more accurately represent urban areas in both years. It's important to note that while soil classes for BSI were determined in the field, the same level of ground truthing was not conducted for NDBI. Therefore, to effectively analyze changes in imperviousness within the watershed resulting from artificial surfaces, emphasis is placed on utilizing the NDVI and BSI indices.

In 2013, a runoff coefficient of 0.755 was obtained for the entire watershed through the assignment of runoff coefficients to land cover and areal weighted average, while in 2022, the runoff coefficient increased slightly to 0.760. In a theoretical scenario without artificial surfaces, the runoff coefficient is around 0.730. It is important to note that the most significant changes in imperviousness were recorded in the middle watershed, where an increase of 205 187 m^2 in artificial surfaces was estimated, as illustrated in Fig. 5.

According to field analysis, the two site points M1 (undisturbed creek) and M2 (channeled creek) show different impervious characteristics, even though they have the same sandy texture. Areas near urbanization or with the presence of shantytowns present a lower infiltration rate (M1: 812 mm/hr) than areas located around undisturbed creeks (M2: 526 mm/hr), mainly due to soil compaction and the presence of impervious surfaces.

In 2013, a maximum flow of 10.8 m^3/s was recorded, while in 2022 this value increased to 10.9 m^3/s , suggesting an increase in flows attributable to the growth of impervious surfaces in the watershed. In the theoretical scenario, which considers only the present natural cover, a maximum flow of 10.4 m^3/s

was recorded. Fig. 6 shows the hydrographs comparison for the theoretical, 2013 and 2022 scenarios with a storm direction towards upstream and downstream.

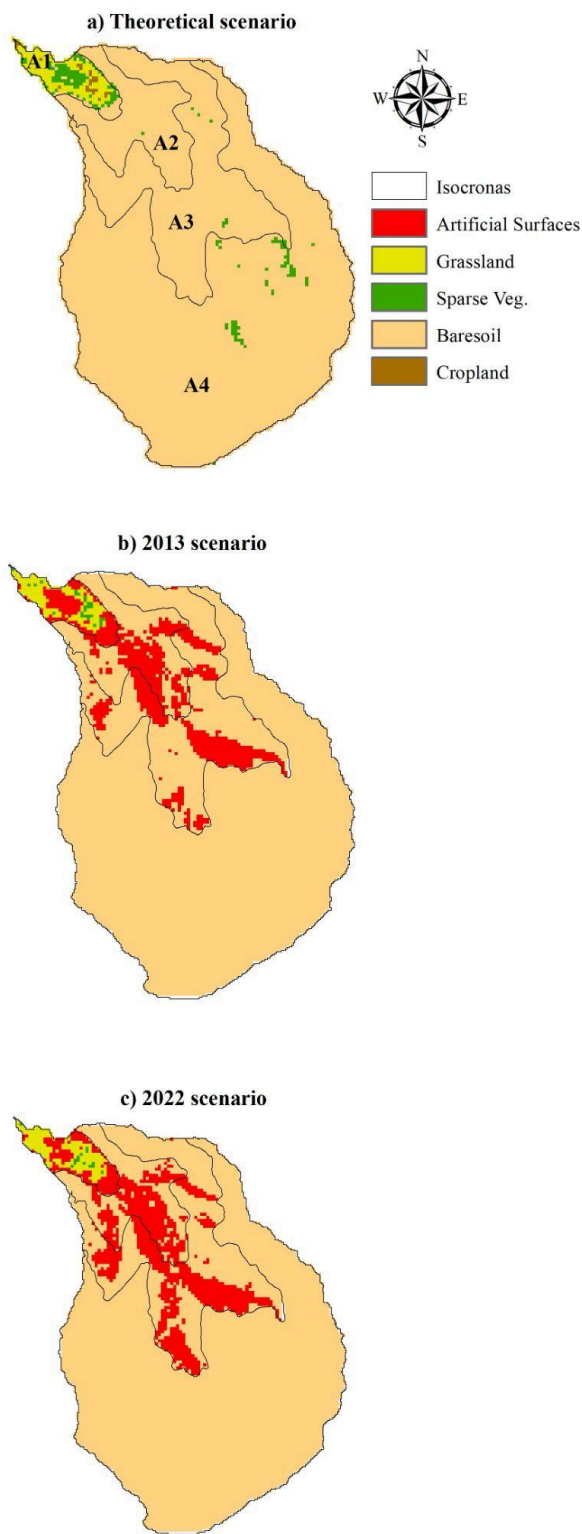


Fig. 5. Land use change with NDVI and BSI indices for 3 scenarios.

To estimate the erosion rate, the LS factor was used, with a spatialized average value of 0.9 for the watershed. Then, the sedimentation rate for the hydrographic network was calculated, obtaining 8 265 t for 2013 and 8 355 t for 2022. This reveals an increase of 90 t in the amount of sediment during storm events. In the theoretical scenario, the sediment rate was 7 848 t per event. Table I shows the comparison of artificial surfaces, peak flows, runoff volumes generated, and erosion rate between the theoretical scenario, the 2013 scenario, and the 2022 scenario.

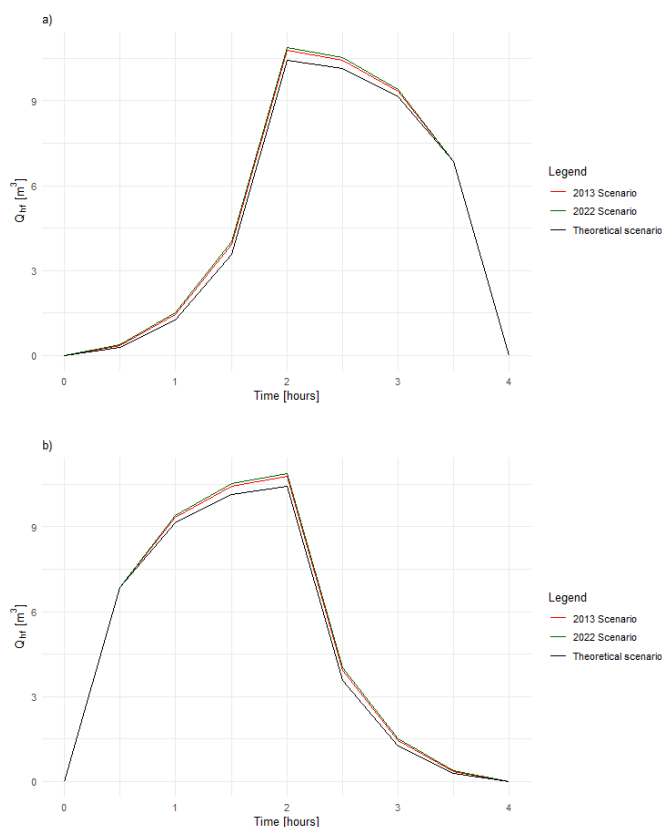


Fig. 6. Hydrographs comparison (a) with a storm direction towards upstream and (b) with a storm direction towards downstream.

TABLE I
FLOW AND EROSION RATES FROM LAND COVER SCENARIO COMPARISON

Scenario	Artificial surface [m ²]	Q _{hf} [m ³ /s]	Volume [m ³]	Erosion [t/event]
Theoretical	0	10.4	112 839	7 848
2013	872946	10.8	116 850	8 265
2022	1078133	10.9	117 983	8 355

The difference in the hydrograph shapes depending on the direction of the storm is shown. A storm in the upstream to downstream direction would present an earlier maximum

event than the event in the reverse direction. This behavior is due to the watershed's high slope and shape.

Between 2013 and 2022, a 23.2% increase in artificial surfaces would cause a 0.93% increase in peak flow. These values are almost identical for event-generated erosion with a 6.5% increase between the 2022 scenario and the theoretical scenario. Although the increase could be considered low, both in flow and sediment produced per event, it should be emphasized that this generated volume would not be adequately evacuated since the lower surfaces of channels or low levels are very impermeable due to paving, compaction, and concrete infrastructure. This would result in the accumulation of the flow and the inadequacy of the hydraulic section for its evacuation to the Rimac River, the main river towards Lima city, which receives hyperconcentrated and debris flows from dry creeks. It causes a population water shortage because of the collapse of treatment plants due to high suspended sediment concentrations.

The use of low-cost monitoring technologies provides relevant information in uninstrumented watersheds such as the California Creek. SENAMHI (National Service of Meteorology and Hydrology of Peru) implemented the tool ISAAC [18]. This open-use tool provides information about precipitation at monitoring stations located in ravines. California Creek has a station that allows the population to be informed about rainfall events in the watershed.

As well, nature-based solutions offer a valuable contribution to hyperconcentrated flood protection by taking advantage of the ecosystem services provided by watersheds, such as native vegetation in lowlands and people's local knowledge. These solutions not only promote biodiversity and disaster prevention but also reduce flood risk by providing tools to control water levels. In addition, they contribute to stream stabilization, and their integration with an interdisciplinary approach will allow more effective adaptation to changing conditions, resulting in less demanding design requirements, such as local knowledge of hyperconcentrated flows and identification of erosion and sedimentation zones.

V. CONCLUSIONS

A 5.1% increase in flow generation considering artificial surfaces (with a level of imperviousness caused by urbanization) is obtained by 2022 with respect to the theoretical scenario without the presence of artificial surfaces. Storm events downstream could be more common, according to local people's experience. According to the obtained hydrograph shapes, this could cause fast runoff event generation due to large contribution areas and high slopes; therefore, any plan or decision for managing flood risk should consider it.

It was identified as a necessity to improve urban planning and a technical-based authorization for urban expansion (i.e., new condominium areas). Our results suggest that risk

identification must consider dry creek and hillside proximity. Any intervention capable of increasing the runoff coefficient significantly will increase the hyperconcentrated flow hazard. Also, the planning and design of small rock dykes, check dams, or riprap dykes for hyperconcentrated flow attenuation must consider monitoring sediment transport through local stations at different scales. These stations allow us to understand how erosion develops in an area and what its main causes are. The successful implementation and sustainable management of these solutions are closely linked to several governance-enabling factors and interrelated concepts. These concepts include stakeholder participation, appropriate policy and management capacity, economic efficiency, synergies and trade-offs, adaptation to local conditions, long-term performance, and appropriate spatial scale.

It is important to highlight that the urbanization process in the California basin should follow guidelines, considering the information provided on the generation of mudflows. The purpose of this is to guarantee orderly urban growth and manage the risk of flood disasters by reducing the vulnerability of the urban areas in the basin.

ACKNOWLEDGMENT

The authors thank the support of the UTEC Research Office, SeHClim: Water security and climate change research group and the help of students of environmental and civil engineering for field work and lab procedures.

REFERENCES

- [1] M. Cordova, P. Rau, L. Bourrel and J. Sosa, "El Niño impacts from large to local scale on Peruvian rivers". Proceedings of the IAHR World Congress. pp. 2927-2936, August 2023. Available: https://dx.doi.org/10.3850/978-90-833476-1-5_iahr40wc-p0407-cd
- [2] A. R. Mejía Uquiche and J. Ronchail, "Risques liés aux écoulements torrentiels et leur gestion à Chosica (Lima, Pérou)", *EchoGéo*, n.º 50, December 2019. Available: <https://doi.org/10.4000/echogeo.18392>
- [3] A. Rasul, H. Balzter, G. Faqe, H. Hameed, J. Wheeler, B. Adamu, S. Ibrahim and P. Najmaddin, "Applying Built-Up and Bare-Soil Indices from Landsat 8 to Cities in Dry Climates", *Land*, vol. 7, n.º 3, p. 81, July 2018. Available: <https://doi.org/10.3390/land7030081>
- [4] P. Fabijańczyk and J. Zawadzki, "Spatial correlations of NDVI and MSAVI2 indices of green and forested areas of urban agglomeration, case study Warsaw, Poland", *Remote Sens. Appl.: Soc. Environ.*, vol. 26, p. 100721, April 2022. Available: <https://doi.org/10.1016/j.rsase.2022.100721>
- [5] Y. Zheng, L. Tang and H. Wang, "An improved approach for monitoring urban built-up areas by combining NPP-VIIRS nighttime light, NDVI, NDWI, and NDBI", *J. Cleaner Prod.*, vol. 328, p. 129488, December 2021. Available: <https://doi.org/10.1016/j.jclepro.2021.129488>
- [6] J. Yang, D. Yan, Z. Yu, Z. Wu, H. Wang, W. Liu, S. Liu and Z. Yuan, "NDVI variations of different terrestrial ecosystems and their response to major driving factors on two side regions of the Hu-Line", *Ecolog.*

- Indicators, vol. 159, p. 111667, February 2024. Available: <https://doi.org/10.1016/j.ecolind.2024.111667>
- [7] D. T. Loi, T.-Y. Chou and Y.-M. Fang, “Integration of GIS and Remote Sensing for Evaluating Forest Canopy Density Index in Thai Nguyen Province, Vietnam”, *Int. J. Environmental Sci. Develop.*, vol. 8, n.º 8, pp. 539–542, 2017. Available: <https://doi.org/10.18178/ijesd.2017.8.8.1012>
- [8] Instituto Geológico, Minero y Metalúrgico (INGEMMET), “Flujos de detritos del 05/04/2012 entre las quebradas La Ronda y Los Condores margen izquierda del río Rimac”. Report A6608, 2012.
- [9] J. Akib, C. Qimin, P. Hao, A. Orhan, L. Yan, A. Iffat, H. Enamul, A. Yeamin and S. Nayyer, “Review of Spectral Indices for Urban Remote Sensing”. *Photogrammetric Engineering & Remote Sensing*, vol 87, n° 7, p. 513-524, July 2021. Available: <https://doi.org/10.14358/PERS.87.7.513>
- [10] J. Latham, R. Cumani, I. Rosati and M. Bloise, “Global Land Cover SHARE (GLC-SHARE) database Beta-Release Version 1.0 - 2014”, 2014.
- [11] Servicio Nacional de Meteorología e Hidrología del Perú SENAMHI-IDESEP, “Módulo para la estimación de curvas de Intensidad-Duración-Frecuencia (IDF)”, 2021. Available: <https://idesep.senamhi.gob.pe/dhi-idf/>
- [12] Instituto Geofísico del Perú (IGP), “Análisis y evaluación histórica de precipitaciones en Chacacayo, Chosica y áreas aledañas”. Report N°001-2023. Peru. p. 115, 2023
- [13] V. P. Singh, “Hydrologic Systems: Rainfall-Runoff Modeling”. vol. 1. EnglewoodCliffs, N.J.: Prentice Hall, 1988.
- [14] P. Rau, L. Gutierrez and N. Callan, “A tool in R for handling hydrologic drainage design”. *Advances in Science, Technology and Innovation*. (in-press), 2024.
- [15] P. Rau, N. Callan, W. Abad and K. Visitacion, “Stormwater Runoff Assessment Under Climate Change Scenarios Using Remote Sensing Products. A Case Study in Piura, Peru”. *Proceedings of the IAHR World Congress*. pp. 7139-7146, June 2022. Available: doi:10.3850/IAHR-39WC2521711920221794
- [16] JR. Williams, “Sediment-yield prediction with universal equation using runoff energy factor. Present and prospective technology for predicting sediment yield and sources”, pp. 244-252, 1975.
- [17] S. Goslee, H. Gall and T. Veith, “VFS: Vegetated Filter Strip and Erosion Model”. v.1.0.2. R CRAN Package, 2022.
- [18] Servicio Nacional de Meteorología e Hidrología del Perú (SENAMHI) and Practical Action, “Monitoreo de lluvias intensas en la región Lima frente a la activación de quebradas”, 2024. Available: <https://app.powerbi.com/view?r=eyJrIjoiMzFIODU4NmItZjcyMi00MD E5LWFhMzgtMDA5ODAzNzVjODcyliwidCI6IjFiMThkODNiLWQxN WYtNDE2YS04NTg2LTY4YjcwYTE0NjRjYSIsImMiOiR9>